American Mineralogist, Volume 87, pages 1458–1463, 2002

The structure of Mn-rich tuperssuatsiaite: A palygorskite-related mineral

FERNANDO CÁMARA,[1,†] LAURENCE A.J. GARVIE,[1,*] BERTRAND DEVOUARD,[1,‡] THOMAS L. GROY,[2] AND PETER R. BUSECK[1,2]

[1]Department of Geological Sciences, Arizona State University, Tempe, Arizona 85287-1404, U.S.A.
[2]Department of Chemistry/Biochemistry, Arizona State University, Tempe, Arizona 85287, U.S.A.

ABSTRACT

The structure of tuperssuatsiaite from the Aris phonolite in central Namibia was refined to an R index of 0.075 for 905 observed reflections [$I > 2\sigma(I)$] obtained with a four-circle X-ray diffractometer. Tuperssuatsiaite is monoclinic, $C2/m$, with $a = 14.034(7)$, $b = 17.841(7)$, $c = 5.265(2)$ Å, and $\beta = 103.67(4)°$. Microprobe analysis gave an average composition of $Na_{1.87}Fe_{2.14}Mn_{0.48}Ti_{0.14}Al_{0.03}Mg_{0.02}[Si_8O_{20}](OH)_2 \cdot n(H_2O)$, with five octahedral sites. The structure is closely related to that of palygorskite $Mg_5[Si_8O_{20}](OH)_2 \cdot H_2O$. Tuperssuatsiaite consists of ribbons of SiO_4 tetrahedra linked by bands of octahedra running parallel to **c**. Channels occur that could be occupied by H_2O as in palygorskite. The octahedral band contains three edge-sharing, six-coordinated sites labeled M1, M2, and M3. This band consists of alternating M3-M1-M3 and M2-M2 octahedra along [001]. The M1 and M2 sites both contain Fe and Mn, and M3 is occupied by Na. Bond-valence calculations indicate a formal charge of 2.48 for M1 and 2.67 for M2, i.e., a charge distribution of $2R^{3+}:1R^{2+}$. Octahedral angle variance and volume are similar for both sites, indicating disorder in the distribution of Fe and Mn atoms between the sites. Charge balance requirements agree with the presence of Fe^{3+} and Mn^{2+}.

INTRODUCTION

Structure determinations of palygorskite and related species, such as tuperssuatsiaite, are limited due to a lack of suitable crystals for single-crystal X-ray diffraction. Understanding these minerals is important for calculating physical and chemical properties such as the number and behavior of channel and surface-molecular exchange sites. Most palygorskite-group minerals crystallize as fine-grained, hair-like aggregates with fiber widths of less than a few microns. Because of these crystallites, structural information has been inferred mostly from powder X-ray diffraction and transmission electron microscopy. As a result, numerous models have been produced regarding cell dimensions and indexing of powder patterns (Christ et al. 1969; Jones and Galan 1988) and polymorphs and structure models (Bradley 1940; Presinger 1963; Zyvagin et al. 1963; Gard and Follet 1968; Drits and Aleksandrova 1966; Drits and Sokolova 1971; Chisholm 1990, 1992).

Tuperssuatsiaite has a diffraction pattern similar to that of palygorskite, which implies that they have related structures. The palygorskite type minerals exhibits a range of structure variations as shown by yofortierite, the Mn-analogue of palygorskite (Perrault et al. 1975); intersilite (Na,K) $Mn(Ti,Nb)Na_5(O,OH)(OH)_2[Si_{10}O_{23}(O,OH)_2] \cdot 4H_2O$ (Egorov-Tismenko et al. 1996; Yamnova et al. 1996), a sepiolite-related mineral; and raite $Na_3Mn_3Ti_{0.25}[Si_8O_{20}](OH)_2 \cdot 10H_2O$ (Pluth et al. 1997), with $Na(H_2O)_6$ octahedra along the channels. Kalifersite $(K,Na)_5(Fe^{3+})_7[Si_{20}O_{50}](OH)_6 \cdot 12H_2O$ was described as a member of the palygorskite-sepiolite series (Ferraris et al. 1996, 1998; Ferraris 1997), with a and c lattice parameters similar to sepiolite and palygorskite and the b parameter intermediate between them.

Tuperssuatsiaite is common in some miarolitic cavities associated with alkaline intrusive and extrusive rocks from the Aris phonolite, Windhoek, Namibia (von Knorring et al. 1992). It was first described from the Ilímaussaq alkaline complex, South Greenland (Karup-Møller and Petersen 1984). We had access to high-quality specimens of tuperssuatsiaite from a new occurrence in the Aris phonolite and located a suitable crystal to perform a single-crystal X-ray diffraction study.

OCCURRENCE

The phonolite intrusion is located about 25 km south of Windhoek. The samples were collected from a quarry being mined for road and railway ballast. The phonolite is highly vesicular, fine grained, aphyric, and consists of alkali feldspars, nepheline, and acmite with minute accessory apatite, zircon, and monazite (von Knorring and Franke 1987; Jahn et al. 2001). The vesicles range from ca. 1 mm to 10 cm in diameter. Many are filled with fluid and appear to burst when the rock is split. In addition to tuperssuatsiaite, the vesicles contain villiaumite, natrolite, aegerine, microcline, apophyllite, analcime, fluorite, kanemite, hydroxyapatite, galena, sphalerite, makatite, quartz, and other less well-characterized or new species. The occurrence and structure of kanemite from the Aris phonolite was recently described (Garvie et al. 1999).

* E-mail: lgarvie@asu.edu
† Present address: CNR-Istituto di Geoscienze e Georisorse, sezione di Pavia, via Ferrata 1, 27100 Pavia, Italy.
‡ Present address: Département de Géologie, UMR 6524 Magmas et Volcans, 5 rue Kessler, F-63038 Clermont-Ferrand cedex, France.

Tuperssuatsiaite is common in most of the miarolitic cavities (D. Shannon, personal communication) and occurs with at least two new isomorphous species. The tuperssuatsiaite occurs as radial aggregates of thin crystals (Fig. 1) ranging from ca. 1 to 10 mm in length, with laths typically <20 μm in width. The color is variable, ranging through various shades of green, red, and brown, even in the same hand specimen. Tuperssuatsiaite commonly grows from a small aggregate of light-brown to green aegerine. The crystals are elongated along [001], with good (100) cleavage. The ends of the crystals are commonly terminated by the {001} basal pinacoid.

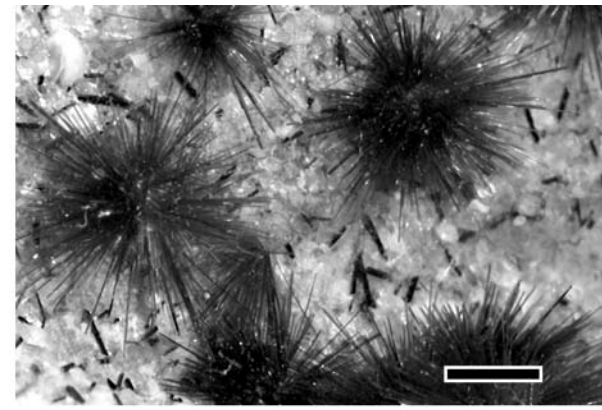

FIGURE 1. Tuperssuatsiaite sprays in a vug. The smaller dark laths are aegerine and the clear crystals are zeolites. The scale bar is 1 mm in length.

EXPERIMENTAL METHODS

Structure refinement

A crystal of tuperssuatsiaite 0.59 × 0.03 × 0.09 mm in size was chosen. X-ray data were acquired using a Siemens *P*3 autodiffractometer employing graphite-monochromatized Mo$K\alpha$ radiation. The crystal was checked for (100) twinning, which is common for these crystals (von Knorring et al. 1992). Unit-cell parameters were refined using 25 independent reflections in the theta range 5.99–13.59°. Details of data collection and results of the structure refinement are given in Table 1. The space group is *C*2/*m*, with 318 ($I > 3\sigma$) observed *C*-centering violations. Atomic scattering curves for fully ionized cations and neutral atoms were employed (Ibers and Hamilton 1974). For the anion positions, both the O^{2-} scattering curve (Tokonami 1965) and neutral scattering curve for O (Ibers and Hamilton 1974) were used and compared for the best fit.

The structure was solved using the SHELXS direct methods software in the SHELXTL PC v. 5.03 commercial package (1994) from Siemens Analytical X-ray Instruments. Anisotropic displacement parameters were refined after all framework O atoms and cations were located. We used both neutral and ionized scattering curves (Si and Si^{4+}) for tetrahedral sites to estimate the formal charges at these sites and to allow for better estimation of their displacement parameters. Finally, to estimate the formal charge at each site and to allow for better estimation of displacement parameters at the O sites, we duplicated those sites, assigning a neutral and an ionized scattering curve to each; we then refined each duplicate site with constrained atom coordinates, anisotropic displacement parameters, and restrained occupancy. Details on this procedure for assigning charge are given in Hawthorne et al. (1995).

A difference-Fourier map showed a residual maximum in the channel that was included in the refinement. This maximum represents low electron density. Although it is insufficient for O, it might arise from an H_2O molecule that is either disordered within the channels or a site with partial H_2O occupancy. Consequently, O9 has a large isotropic displacement parameter, which may account for the weak cell-centering violations. Table 2 lists the atomic coordinates and the displacement parameters. Selected bond distances and angles are given in Table 3. Observed and calculated structure factors are given in Table 4[1].

TABLE 1. Crystal data and structure-refinement for tuperssuatsiaite

Crystal size	0.59 × 0.03 × 0.09 mm
Wavelength	0.71073 Å
Crystal system, space group	Monoclinic, *C*2/*m*
Unit-cell dimensions	a = 14.034(7) Å, α = 90°
	b = 17.841(7) Å, β = 103.67(4)°
	c = 5.265(2) Å, γ = 90°
V	1280.9(9) Å^3
Z	4
F(000)	881
Range for data collection	1.88 to 25.05°
Index ranges	$-16 \le h \le 16$, $-21 \le k \le 21$, $-6 \le l \le 6$
Reflections collected/unique	2468/1184 (R_{int} = 0.0360)
Refinement method	Full-matrix least-squares on F^2
Data/restraints/parameters	1184/12/125
Goodness-of-fit on F^2	1.136
Final R indices [$I > 2\sigma(I)$]	$R1$ = 0.0748, wR^2 = 0.1977
R indices (all data)	$R1$ = 0.0959, wR^2 = 0.2110
Extinction coefficient	0.0008(7)
Largest difference peak and hole	2.122 and –0.549 e$^-$/Å^3

Electron microprobe (EMP) and transmission electron microscopic (TEM) analyses

Tuperssuatsiaite crystals were embedded in epoxy resin, polished, and analyzed with a JEOL 8700 JXA Superprobe with wavelength dispersive spectrometers, using beam conditions of 15 kV and 10 nA (Table 5). These crystals were obtained from the same vug that produced the crystal for structure determination. The following natural minerals and synthetic materials were used as standards: Durango apatite (F), NaCl (Cl), quartz (Si), synthetic Al_2O_3 (Al; O), synthetic MgO (Mg), Amelia albite (Na), wollastonite (Ca), orthoclase OR1 (K), rutile (Ti), synthetic fayalite (Fe), rhodonite (Mn), and barite (Ba). Na and K were analyzed first for 10 s to minimize the effects of beam damage. The data were processed with standard ZAF data correction procedures.

Several crystals were crushed in methanol, and a drop of the mineral in suspension was dried on a Cu TEM grid coated with lacey amorphous C. Selected-area electron diffraction (SAED) patterns were recorded with a JEOL 2000fx TEM operated at 200 kV.

[1]For a copy of Table 4, document item AM-02-018, contact the Business Office of the Mineralogical Society of America (see inside front cover of recent issue) for price information. Deposit items may also be available on the American Mineralogist web site at http://www.minsocam.org.

TABLE 2. Atom coordinates ($\times 10^4$), equivalent isotropic displacement parameters ($Å^2 \times 10^3$), and anisotropic displacement parameters ($Å^2 \times 10^3$) for tuperssuatsiaite

Atom	Site occ.	x	y	z	U_{eq}	U_{11}	U_{22}	U_{33}	U_{23}	U_{13}	U_{12}
T1		2974(2)	4158(1)	366(5)	16(1)	19(1)	13(1)	16(1)	0(1)	6(1)	–3(1)
T2		2962(2)	3327(1)	5301(4)	17(1)	22(1)	16(1)	13(1)	–1(1)	5(1)	–5(1)
M1	Fe 0.43(1)	5000	5000	0	14(1)	21(1)	11(1)	13(1)	0	7(1)	0
	Mn 0.57(1)										
M2	Fe 0.33(2)	5000	4095(1)	5000	15(1)	15(1)	18(1)	13(1)	0	3(1)	0
	Mn 0.67(2)										
M3	Na 0.94(1)	5000	2970(3)	0	29(2)	30(4)	32(4)	21(3)	0	–2(2)	0
O1		4154(4)	4164(3)	1216(11)	17(1)	19(3)	17(3)	17(3)	–2(2)	9(3)	–1(3)
O2		4120(5)	3333(4)	5920(11)	22(2)	25(3)	26(4)	16(3)	–1(3)	8(3)	1(3)
O3		2500	2500	5000	31(2)	46(6)	19(5)	30(5)	0(4)	13(4)	–13(5)
O4		5699(7)	5000	3767(16)	20(2)	27(5)	15(4)	18(4)	0	6(4)	0
O5		2539(7)	5000	–55(19)	22(2)	21(5)	13(4)	31(5)	0	2(4)	0
O6		2515(4)	3766(4)	2581(11)	21(2)	18(3)	27(4)	21(3)	2(3)	9(3)	0(3)
O7		2563(4)	3716(4)	7655(12)	23(2)	21(3)	23(3)	25(4)	–4(3)	7(3)	–6(3)
O8		4291(10)	2048(8)	2068(3)	103(5)	95(9)	112(10)	115(10)	–27(9)	51(8)	–60(8)
O9		5560(6)	0	2902(15)	500(5)						

Note: U_{eq} is defined as one third of the trace of the orthogonalized U_{ij} tensor. The anisotropic displacement factor exponent takes the form: $-2\pi^2 [h^2 a^{*2} U_{11} + ... + 2 h k a^* b^* U_{12}]$. Atom O9 refined as isotropic.

TABLE 3. Selected interatomic distances (Å) and angles (°), and selected derived parameters for tuperssuatsiaite

T1-O1	1.610(7)	M1-O1 (×4)	2.098(6)
T1-O5	1.617(4)	M1-O4 (×2)	1.994(9)
T1-O6	1.618(6)	<M1-O>	2.064
T1-O7[f]	1.613(6)	V(Å^3)	11.528
<T1-O>	1.615	OAV	36.217
V(Å^3)	2.157	OQE	1.0115
TAV	5.596		
TQE*	1.0013	M2-O1 (×2)	2.068(6)
		M2-O2 (×2)	1.973(6)
O1-T1-O5	111.3(4)	M2-O4 (×2)	2.072(6)
O1-T1-O7[f]	112.2(3)	<M2-O>	2.038
O1-T1-O6	111.2(3)	V(Å^3)	11.097
O5-T1-O6	107.3(4)	OAV	35.314
O5-T1-O7[f]	106.8(4)	OQE	1.0111
O6-T1-O7[f]	107.8(3)		
		M3-O1 (×2)	2.592(8)
T2-O2	1.580(7)	M3-O2[d] (×2)	2.303(6)
T2-O3	1.604(2)	M3-O8 (×2)	2.322(13)
T2-O6	1.623(6)	<M3-O>	2.406
T2-O7	1.631(6)	V(Å^3)	16.686
<T2-O>	1.610	OAV	256.199
V(Å^3)	2.134	OQE	1.0770
TAV	8.580		
TQE*	1.0021		
O2-T2-O2	111.2(3)		
O2-T2-O3	113.5(3)		
O2-T2-O6	110.0(3)		
O3-T2-O6	107.1(3)		
O3-T2-O7	105.2(3)		
O6-T2-O7	109.5(3)		
T2[h]-O3-T2	180.0		
T1[c]-O5-T1	136.6(6)		
T1-O6-T2	135.0(4)		
T1[g]-O7-T2	139.9(4)		
O5-O6-O7	124.3(4)		
O6-O5-O6	115.2(4)		
O7-O5-O7	124.2(4)		
O6-O7-O5	115.9(4)		
O7-O6-O7	175.1(4)		

Notes: TAV = tetrahedral angle variance; TQE = tetrahedral quadratic elongation; OAV = octahedral angle variance; OQV = octahedral quadratic elongation. Symmetry transformations used to generate equivalent atoms: a = $-x+1, -y+1, -z$; b = $-x+1, y, -z$; c = $x, -y+1, z$; d = $-x+1, y, -z+1$; e = $-x+1, -y+1, -z+1$; f = $x, y, z-1$; g = $x, y, z+1$; h = $-x+1/2, -y+1/2, -z+1$V.

* Following Robinson et al. (1971).

RESULTS AND DISCUSSION

The structure of tuperssuatsiaite was solved and refined to an R index of 0.075 for 905 reflections [$I > 2\sigma(I)$] in space group $C2/m$ with $a = 14.034(7)$, $b = 17.841(7)$, $c = 5.265(2)$ Å, and $\beta = 103.67(4)°$. Microprobe analysis gave an average composition of $Na_{1.87}Fe_{2.14}Mn_{0.48}Ti_{0.14}Al_{0.03}Mg_{0.02}[Si_8O_{20}](OH)_2 \cdot n(H_2O)$.

In addition to reflections consistent with space group $C2/m$, there were 318 weak reflections, with $I > 3\sigma$ representing C-centering violations. The data set does not allow us to distinguish between $C2/m$ or $P2_1/m$ space groups. The solutions of the structure in space group $P2_1/m$ showed the same topology but with four unique tetrahedral sites and double the number of anion sites. The inner angles of the tetrahedral rings and O7-O6-O7 angle are similar. However, owing to the low $I/\sigma I$ ratio of the hkl reflections with $h + k = 2n + 1$, the R factor after least-squares refinement was twice that for space group $C2/m$, and the associated errors on distances and angles were equally higher. The loss of C centering may be caused by partially occupied but ordered H_2O along the channels. Electron-diffraction data (Fig. 2) supports this interpretation because weak $h + k = 2n + 1$ reflections are present.

We also refined models in space groups $C2$ and Cm, which have the same extinction conditions as $C2/m$. For $C2$ and Cm, the R values were lower, 0.066 and 0.075, respectively. However, some O sites refined to non-positive definite thermal ellipsoids. In addition, the distributions of the intensities of reflections were consistent with a centrosymmetric space group (using the routine ADDSYM incorporated in PLATON; Spek 2001). Refinement in Cm revealed missing additional symmetry compatible with space group $C2/m$. Following the recommendations of Marsh (1995), we decided to use the $C2/m$ space group.

The tuperssuatsiaite structure consists of an octahedral sheet sandwiched between two opposing tetrahedral sheets. The octahedral sheet forms strips that are three octahedra wide (Fig. 3a). In mica, the tetrahedral sheet consists of unbranched zweier single layers, and the apical O atoms of each SiO_4 unit point in the same direction. This sheet is modified in tuperssuatsiaite (and palygorskite) in that the apical O atoms of adjacent zweier chains lie on opposite sides of the sheets (Fig. 3a). The

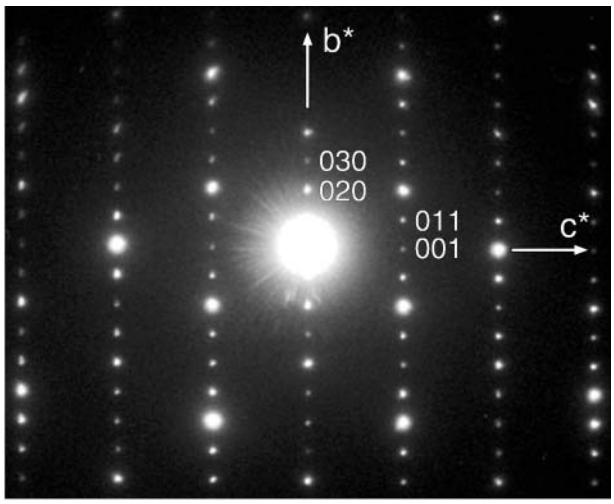

FIGURE 2. [100] zone axis SAED pattern of tuperssuatsiaite.

tuperssuatsiaite structure may also be described by building blocks or "I-beams" similar to those of clinoamphiboles. A **c**-axis projection (Fig. 3b) shows the corrugated sheets of SiO_4 tetrahedra that are linked by ribbons of Na, Fe, and Mn octahedra.

X-ray single-crystal refinement and microprobe results are consistent with 8 Si at the tetrahedral sites per 21(O + OH). There is no substitution of the form $^{[IV]}$Si-Al. Aluminum concentrations are low (Table 5), and bond distances of both tetrahedral sites agree with full Si occupancy. The T2 site is more deformed than the T1 site (Table 3), as indicated by its higher tetrahedral angle variance (TAV). The T2 site is deformed because the O atoms at this site join adjacent "I-beams" (Fig. 3b). The T2-O3-T2 angle is constrained by symmetry to be 180° (O3 atoms are on a special position), as is the case for raite. This bond joins adjacent I beams, thus forming a stressed T2-O3 bond and explaining the large displacement factor for O3 (Table 3).

Every double silicate chain forms hexagonal rings of tetrahedra (Fig. 3a) that deviate only slightly from ideality (120°). The angular distortion parameter α (Radoslovich 1961) shows a low deviation of 2.1. There is no tetrahedral substitution in tuperssuatsiaite, and therefore the slight distortion of the hexagonal arrangement is caused by matching requirements between tetrahedral apices and the octahedral layer.

The octahedral band contains three unique edge-sharing, six-coordinated sites M1, M2, and M3. This band consists of alternating M3-M1-M3 and M2-M2 octahedra along [001] (Fig. 3a). M1 is nearly fully occupied. The equivalent site in palygorskite is described as empty (Serna et al. 1977; Güven et al. 1992; Grobety et al. 1995), although it is also reported to be partially occupied and forming a series between dioctahedral and trioctahedral palygorskites (Jones and Galan 1988). The extent of M1 occupancy probably depends on the valence of the other octahedral cations. The M3 site is occupied by Na. This monovalent cation allows entry of trivalent and tetravalent (e.g., Ti^{4+}) cations into the M1 and M2 sites when there is not simultaneous $^{[IV]}$Si-Al substitution. EMP analyses show a small octahedral-cation deficiency (M1 + M2 = 2.82 atoms per formula unit).

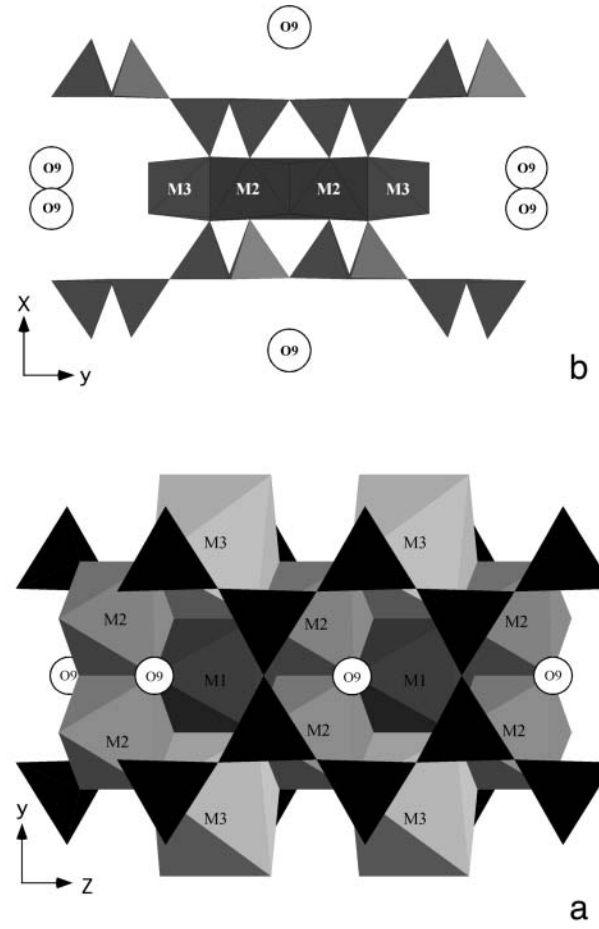

FIGURE 3. The structure of tuperssuatsiaite projected (**a**) along [100] and (**b**) along [001].

Bond-valence calculations (Eutax v. 1.5 program, Brese and O'Keeffe 1991) were performed for the theoretical Fe-tuperssuatsiaite end-member. The Eutax v. 1.5 program does not allow for partial occupancy in a single site. Therefore, calculations were performed with only one species at the M1 and M2 sites. Since the EMP analysis yielded Mn/(Mn + Fe) <0.5, we decided to perform bond-valence calculations using an Fe-rich end-member (Table 6). The calculations indicate a formal charge of 2.48 for M1 and 2.67 for M2, consistent with a charge distribution of $2R^{3+}$:$1R^{2+}$ at the M1 and M2 sites. The octahedral angle variance (OAV; Robinson et al. 1971) and the M1- and M2-site volumes are consistent with Fe, Mn disorder between these sites. The mean bond length of M1 (<M1-O>; 2.064 Å, Table 3) shows that it is too small to be occupied only by Fe^{2+}. However, <M1-O> is greater than expected for full Fe^{3+} or Mn^{3+} occupancy (2.025 and 2.010 Å, respectively). Therefore, M1 probably contains both divalent and trivalent cations. The volume of the M2 site is slightly smaller than the M1 site and according to the bond-valence calculations the atom has a greater charge. Because Ti^{4+} is smaller than Fe^{3+} or Mn^{3+}, the analyzed 0.1–0.2 Ti atoms per formula unit is probably ordered at the M2 site. This pattern of ordering provides additional

TABLE 5. Chemical composition from EMP analyses

Analysis	1	2	3	4	5	6	7	8	9	10	11	mean	sd
SiO_2	57.267	57.374	57.225	57.588	51.064	56.668	54.273	56.711	56.540	55.684	55.577	55.998	1.908
Al_2O_3	0.019	0.019	0.038	0.265	0.227	0.340	0.113	0.057	0.208	0.397	0.208	0.172	0.132
TiO_2	1.751	1.668	1.068	1.518	0.484	1.284	1.451	1.535	1.351	0.751	1.818	1.334	0.418
FeO	15.322	18.011	11.759	19.851	12.801	20.263	19.915	20.070	20.263	20.507	17.664	17.857	3.177
MnO	6.549	4.345	10.038	2.399	7.211	1.984	1.414	2.308	1.375	1.880	3.839	3.940	2.845
MgO	0.050	0.050	0.099	0.033	0.182	0.050	0.133	0.133	0.149	0.050	0.083	0.092	0.050
CaO	0.042	0.028	0.000	0.028	0.084	0.056	0.028	0.000	0.028	0.042	0.056	0.036	0.025
K_2O	0.060	0.108	0.000	0.349	0.072	0.398	0.120	0.205	0.157	0.096	0.060	0.148	0.124
Li_2O	0.000	0.000	0.000	0.000	0.000	0.000	0.000	0.000	0.000	0.000	0.000	0.000	0.000
Na_2O	6.710	6.266	6.831	4.878	5.686	5.322	7.586	6.791	7.990	8.031	7.640	6.703	1.075
F	0.200	0.190	0.140	0.150	0.200	0.200	0.240	0.170	0.200	0.170	0.210	0.188	0.029
Cl	0.030	0.020	0.040	0.000	0.000	0.000	0.020	0.030	0.000	0.020	0.030	0.017	0.015
H_2O*	2.028	2.036	2.039	2.050	1.792	2.003	1.925	2.031	2.028	2.010	1.989	1.994	0.075
TOTAL	90.029	90.115	89.276	89.109	79.802	88.568	87.218	90.040	90.288	89.638	89.174	88.478	3.009
O = F,CL	0.09	0.08	0.06	0.06	0.08	0.08	0.10	0.07	0.08	0.07	0.09	0.080	0.012
Total	89.94	90.03	89.22	89.05	79.72	88.48	87.12	89.97	90.20	89.57	89.08	88.398	3.012
Si	8.05	8.07	8.10	8.13	8.11	8.09	7.96	8.02	7.98	7.96	7.94	8.038	0.069
Al	0.00	0.00	0.01	0.04	0.04	0.06	0.02	0.01	0.03	0.07	0.04	0.029	0.022
Ti	0.19	0.18	0.11	0.16	0.06	0.14	0.16	0.16	0.14	0.08	0.20	0.143	0.043
Fe	1.80	2.12	1.39	2.34	1.70	2.42	2.44	2.37	2.39	2.45	2.11	2.140	0.360
Mn	0.78	0.52	1.20	0.29	0.97	0.24	0.18	0.28	0.16	0.23	0.46	0.482	0.353
Mg	0.01	0.01	0.02	0.01	0.04	0.01	0.03	0.03	0.03	0.01	0.02	0.020	0.012
S M1 + M2	2.78	2.82	2.74	2.84	2.81	2.87	2.83	2.85	2.77	2.84	2.82	2.815	0.039
Ca	0.01	0.00	0.00	0.00	0.01	0.01	0.00	0.00	0.00	0.01	0.01	0.006	0.004
K	0.01	0.02	0.00	0.06	0.01	0.07	0.02	0.04	0.03	0.02	0.01	0.027	0.022
Na	1.83	1.71	1.88	1.34	1.75	1.47	2.16	1.86	2.19	2.23	2.12	1.865	0.292
S M3	1.85	1.73	1.88	1.40	1.78	1.55	2.18	1.90	2.22	2.25	2.14	1.898	0.278
F	0.09	0.08	0.06	0.07	0.10	0.09	0.11	0.08	0.09	0.08	0.09	0.086	0.014
OH	1.90	1.91	1.93	1.93	1.90	1.91	1.88	1.92	1.91	1.92	1.90	1.910	0.014
Cl	0.01	0.00	0.01	0.00	0.00	0.00	0.00	0.01	0.00	0.00	0.01	0.004	0.004
S (F,OH,Cl)	2.000	2.000	2.000	2.000	2.000	2.000	2.000	2.000	2.000	2.000	2.000	2.000	0.000
S CAT	12.68	12.62	12.72	12.38	12.70	12.51	12.96	12.76	12.97	13.05	12.91	12.751	0.206

Notes: Unit-formula recalculation on the basis of 21(O + OH). All analyses are from crystals situated within the same vug as the crystal used for the structure refinement.
* Calculated by stoichiometry.

charge stability to the local environment because the M3 site shares two edges with two M2 sites and one edge with an M1 site.

Refined site multiplicity parameters indicate fewer than 11 electrons per site for the M3 octahedron (Table 3). The EMP analyses indicate less than two Na atoms per formula unit, which may be caused by devolatization during the analysis, although a defocused beam (25 μm) was used to minimize Na loss. In addition, the Na deficiency as determined by EMP analyses is approximately equal to that obtained from the calculated multiplicity parameter. However, bond-valence calculations for this site indicate a formal charge of 1.24, which may be related to the concentration of Mg in the M3 site, as in palygorskite (Güven et al. 1992). The Mg compensates for the higher formal charge but not for the lower refined site parameter, and therefore some vacancies may be present at the M3 site.

Bond-valence calculations indicate that the O8 site is strongly underbonded and the O4 site less so (Table 6). Unlike palygorskite and raite, in tuperssuatsiaite the O4 and O8 sites are probably occupied by OH groups. However, H does not provide sufficient charge to compensate for the underbonded character of the O8 site as indicated by the bond-valence calculations. On the basis of these calculations and geometrical requirements, the O8 site probably contains an H_2O molecule, thus accounting for the large displacement parameters reported in Table 2. Refinement of the O8 site yielded nearly complete occupancy. One O-H vector of the H_2O molecule points toward O7, with the O atom at the O7 site acting as a donor to provide additional bonding to the tetrahedral sheet, e.g., 08-H···O7 (O8-O7 = 2.971 Å). The other O-H vector projects into the channels.

TABLE 6. Bond-valence calculations for tuperssuatsiaite

	T1	T2	M1	M2	M3	S
O1	1.038		0.373 ×4	0.406 ×2	0.118 ×2	1.935
O2		1.126		0.527 ×2	0.256 ×2	1.909
O3		1.056 ×2→				2.111
O4			0.495 ×2	0.401 ×2		1.296
O5	1.019					2.039
O6	1.015	1.002				2.017
O7	1.028	0.982				2.010
O8					0.244 ×2	0.244
S	4.100	4.166	2.482	2.668	1.236	

Note: Multipliers referring to coordination apply for summations going down the columns. Only for the O3-T2 bond-valence does the multiplier apply for the summation across the table as indicated by the arrow.

Unit-cell parameters for tuperssuatsiaite and minerals with related structures display a range of values. This range is partly related to the difficulty of accurately determining cell parameters from powder data (Chisholm 1992; Artioli et al. 1994). Nevertheless, a plot of lattice parameters of palygorskite (Grobéty et al. 1995), raite (Pluth et al. 1997), and tuperssuatsiaite (Karup-Møller and Petersen 1984; von Knorring et al. 1992) vs. cation ionic radii of M1 + M2 illustrates that the **a** axis length and β angle show a near linear trend (Fig. 4). In contrast, the **b** and **c** axis lengths do not show such a trend. Thus, the length of the **a** axis increases with <*r*> as the octahedral strip thickens as a result of cation substitutions. Simultaneously, the β angle decreases as <*r*> increases. There is a differential displacement between the tetrahedral sheets and a decrease in β to account for the increase in the length of the **a** axis.

ACKNOWLEDGMENTS

We thank D. Shannon for donating samples for this study. This work was supported by the National Science Foundation grants NSF EAR-0003533 and EAR-9418206. We are grateful to the reviewers S. Guggenheim, J. Post, and R. Downs for their helpful comments and suggestions.

REFERENCES CITED

Artioli, G., Galli, E., Burattini, E., Cappuccio, G., and Simeoni, S. (1994) Palygorskite from Bolca, Italy—a characterization by high- resolution synchrotron-radiation powder diffraction and computer modeling. Neues Jahrbuch für Mineralogie Monatshefte, 5, 217–229.

Bradley, W.F. (1940) The structural scheme of attapulgite. American Mineralogist, 25, 405–410.

Brese, N.E. and O'Keeffe, M. (1991) Bond-valence parameters for solids. Acta Crystallographica, B47, 192–197.

Chisholm, J.E. (1990) An X-ray powder-diffraction study of palygorskite. Canadian Mineralogist, 28, 329–339.

———(1992) Powder-diffraction patterns and structural models for palygorskite. Canadian Mineralogist, 30, 61–73.

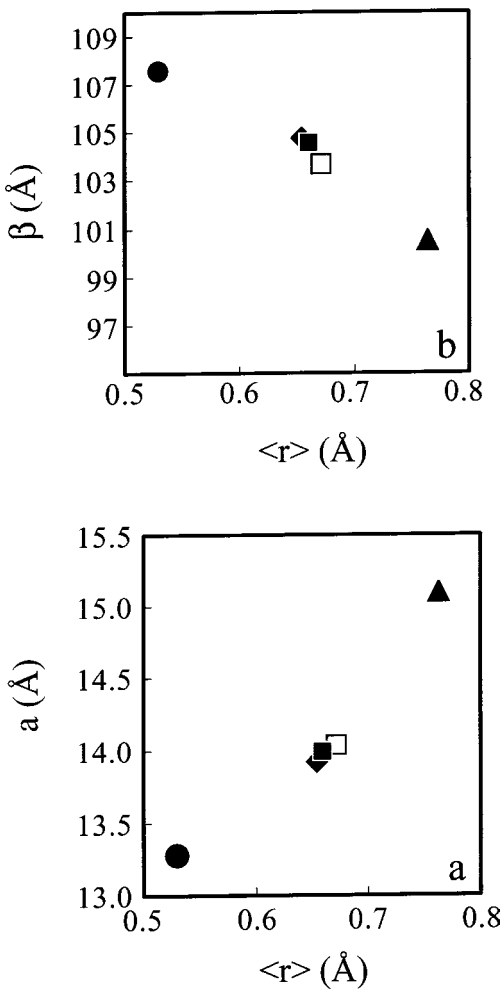

FIGURE 4. Lattice parameter (**a**) *a* and (**b**) β vs. the average ionic radii (<*r*>) in the M1 + M2 sites for tuperssuatsiaite compared with data for raite, palygorskite, and tuperssuatsiaite. Symbols as follows: full dot = palygorskite, Grobéty et al. (1995); full triangle = raite, Pluth et al. (1997); full diamond = tuperssuatsiaite, von Knorring et al. (1992); full box = tuperssuatsiaite, Karup-Møller and Petersen (1984); open box = Aris phonolite, this study (ionic radii are from Shannon 1976).

Christ, C.L., Hathaway, J.C., Hostetler, P.B., and Shepard, A.O. (1969) Palygorskite: new X-ray data. American Mineralogist, 54, 198–205.

Drits, V.A. and Aleksandrova, V.A. (1966) The crystallochemical nature of palygorskites. Zapiski Vsesoyuznovo Mineralogicheskovo Obshchestva, 95, 551–560.

Drits, V.A. and Sokolova, G.V. (1971) Structure of palygorskite. Soviet Physics Crystallography, 16, 183–185.

Egorov-Tismenko, Yu.K., Yamnova, N.A., and Khomyakov, A.P. (1996) A new representative of a series of chain-sheet silicates with inverted tetrahedral fragments. Crystallographic Reviews, 41, 784–788.

Ferraris, G. (1997) Polysomatism as a tool for correlating properties and structure. In S. Merlino, Ed., Modular aspects in minerals. EMU Notes in Mineralogy, 1, 275–295.

Ferraris, G., Khomyakov, A.P., Soboleva, S.V., Belluso, E., and Pavese, A. (1996) Nafertisite, a layer titanosilicate member of a polysomatic series including mica. European Journal of Mineralogy, 8, 241–249.

Ferraris, G., Khomyakov, A.P., Belluso, E., and Soboleva, S.V. (1998) Kalifersite, a new alkaline silicate from Kola Peninsula (Russia) based on a palygorskite-sepiolite polysomatic series. European Journal of Mineralogy, 10, 865–874.

Gard, J.A. and Follet, E.A.C. (1968) A structural scheme for palygorskite. Clay Minerals, 7, 367–370.

Garvie, L.A.J., Devouard, B., Groy, T.L., Camara, F., and Buseck, P.R. (1999) Crystal structure of kanemite, $NaHSi_2O_5 \cdot 3H_2O$, from the Aris phonolite, Namibia. American Mineralogist, 84, 1170–1175.

Grobéty, B., Post, J.E., and Ross, D.R. (1995) Combined TEM/AEM and powder X-ray diffraction study of palygorskite. Terra Abstract, 7, 289.

Güven, N., de la Caillerie, J.B.E., and Fripiat, J.J. (1992) The coordination of aluminum ions in the palygorskite structure. Clays and Clay Minerals, 40, 457–461.

Hawthorne, F.C., Ungaretti, L., and Oberti, R. (1995) Site populations in minerals: terminology and presentation of results of crystal-structure refinement. Canadian Mineralogist, 33, 907–911.

Ibers, J.A. and Hamilton, W.C., Eds. (1974): International Tables for X-ray Crystallography. IV. The Kynoch Press, Birmingham, U.K.

Jahn, S., Medenbach O., Niedermayr, G., and Schneider, G. (2001) Namibia. Zauberwelt elder Steine und Kristalle. Ein praktischer Ratgeber zum Entdecken, Bestimmen, und Sammeln in Namibia. Rainer Bode Gedruckt, Germany.

Jones, B.F. and Galan, E. (1988) Sepiolite and Palygorskite. In S.W. Bailey, Ed., Hydrous Phyllosilicates. Reviews in Mineralogy, 19, 631–674.

Karup-Møller, S. and Petersen, O.V. (1984) Tuperssuatsiaite, a new mineral species from the Ilímaussaq intrusion in South Greenland. Neues Jahrbuch für Mineralogie Monatshefte, 501–512.

Marsh, J.S. (1987) Evolution of a strongly differentiated suite of phonolites from the Klinghardt Mountains, Namibia. Lithos, 20, 41–58.

Perrault, G., Harvey, Y., and Pertsowsky, R. (1975) La yoforterite, un nouveau silicate hydraté de manganèse de St.-Hilaire, P.Q. Canadian Mineralogist, 13, 68–74.

Presinger, A. (1963) Sepiolite and related compounds: its stability and application. Clay and Clay Minerals, 10, 365–371.

Pluth, J.J., Smith, J.V., Pushcharovsky, D.Y., Semenov, E.I., Bram, A., Riekel, C., Weber, H.P., and Broach, R.W. (1997) Third-generation synchrotron x-ray diffraction of 6-μm crystal of raite, approximate to $Na_3Mn_3Ti_{0.25}Si_8O_{20}(OH)_2 \cdot 10H_2O$, opens up new chemistry and physics of low- temperature minerals. Proceedings of the National Academy of Sciences of the United States of America, 94, 12263–12267.

Radoslovich, E.W. (1961) Surface symmetry and cell dimensions of layer silicates. Nature, 191, 67–68.

Robinson, K., Gibbs, G.V., and Ribbe, P.H. (1971) Quadratic elongation: a quantitative measure of distortion in coordination polyhedra. Science, 172, 567–570.

Serna, C., van Scoyoc, G.E., and Ahlrichs, J.L. (1977) Hydroxyl groups and water in palygorskite. American Mineralogist, 62, 784–792.

Shannon, R.D. (1976) Revised effective ionic radii and systematic studies of interatomic distances in halides and chalcogenides. Acta Crystallographica, A32, 751–767.

Tokonami, M. (1965) Atomic scattering factors for O^{2-}. Acta Crystallographica, 19, 486.

von Knorring, O. and Franke, W. (1987) A preliminary note on the mineralogy and geochemistry of Aris phonolite, SWA/Namibia. Communications of the Geological Survey of S.W. Africa (Namibia), 3, 61.

von Knorring, O., Petersen, O.V., Karup-Møller, S., Leonardensen, E.S., and Condliffe, E. (1992) Tuperssuatsiaite, from Aris phonolite, Windhoek, Namibia. Neues Jahrbuch für Mineralogie Monatshefte, 145–152.

Yamnova, N.A., Egorov-Tismenko, Yu.K., and Khomyakov, A.P. (1996) Crystal structure of a new natural (Na,Mn,Ti)-phyllosilicate. Crystallographic Reviews, 42, 239–244.

Zyvagin, B.B., Mishchenko, K.S., and Shitov, V.A. (1963) Electron diffraction data the structures of sepiolite and palygorskite. Soviet Physics Crystallography, 8, 148–153.

MANUSCRIPT RECEIVED MARCH 13, 2001
MANUSCRIPT ACCEPTED JUNE 19, 2002
MANUSCRIPT HANDLED BY JEFFREY E. POST